

Far ultraviolet remote sensing of the isotropy boundary and magnetotail stretching

C. Blockx, J.-C. Gérard, M. Meurant, B. Hubert, and V. Coumans

Laboratoire de Physique Atmosphérique et Planétaire, Université de Liège, Liège, Belgium

[1] Several studies have attempted to identify the isotropy boundary (IB) defining the limit between the adiabatic and nonadiabatic trajectories of the trapped protons along closed magnetic field lines. This boundary is an indicator of the amount of magnetic field line stretching in the magnetotail. Previous studies were based on in situ measurements, resulting in spatially and temporally restricted samples. To overcome these limitations, we propose to use global data obtained with the FUV spectrographic proton auroral imager (SI12) on board the IMAGE satellite. We determine at each magnetic local time the position of an optical boundary related to the IB and thereby to the stretching of the magnetic field lines. We show that the correspondence between the latitude of the maximum proton precipitation observed by SI12 and the IB measured by Defense Meteorological Satellite Program satellites is statistically established and depends on the magnetic local time. The relation between the position of the maximum proton precipitation as well as the intensity of this maximum and the magnetic field distortion is determined by comparison with GOES 8 data. We suggest that SI12 images can be used as a tool to globally determine the isotropy boundary and to monitor the level of stretching in the magnetotail.

1. Introduction

[2] The isotropy boundary (IB) introduced by *Sergeev et al.* [1983] is the low-altitude signature of the transition from the region of the magneto sphere dominated by strong pitch angle scattering to the region of bounce-trapped particles. This transition marks the equatorward boundary of significant ion precipitation. Equatorward of this boundary, the ion distribution function is isotropic outside the mostly empty upgoing and downgoing loss cones. Since the location of the IB is controlled by the magnetic field in the current sheet, the IB position reflects changes in the equatorial magnetic field in the near tail and can be used to monitor these changes. The latitude of this boundary depends on the energy of the particles [*Sergeev et al.*, 1983], with the lower latitudes associated with the highest energies. The IB is well identified from in situ measurements with low-altitude polar spacecraft such as NOAA and FAST satellites. When these spacecraft cross the auroral oval, they provide intensity inside and outside the loss cone. Direct determination of this boundary is not possible from the Defense Meteorological Satellite Program (DMSP) satellites because of the lack of pitch angle coverage (only precipitation fluxes are measured). However, *Newell et al.* [1998] showed a close association between the IB of 30 keV protons detected with NOAA satellites and the b2i boundary defined as the latitude of the ion energy flux precipitation maximum of 3-30 keV protons observed with the DMSP satellites.

[3] The knowledge of the latitude of this boundary in the nightside proton precipitation provides considerable information on the state of the magnetosphere, as it is an indicator of the level of magnetic field line stretching in the magnetotail. Actually, *Sergeev and Gvozdevsky* [1995] showed that unlike geomagnetic indices such as K_p , the magnetotail (MT) index, defined as the invariant latitude of the isotropy boundary of ~ 100 keV protons reduced to the midnight meridian, displays a good correlation ($r \sim 0.9$) with the inclination of the magnetic field measured in the nightside portion of a geosynchronous orbit.

[4] Ground-based remote sensing of the IB location was described by *Donovan et al.* [2003] and *Nicholson et al.* [2002]. *Donovan et al.* [2003] used ion data from DMSP overflights of the Canadian Auroral Network for the OPEN Program Unified Study (CANOPUS) meridian scanning photometer (MSP) located at Gillam, Canada, to develop a simple algorithm to identify the "optical b2i boundary" in latitude profiles of proton auroral (486 nm) brightness. They found by intercomparison of ~ 1600 near-simultaneous optical and in situ b2i that the optical b2i is a reasonable basis for an optical equivalent to the MT index put forward by *Sergeev and Gvozdevsky* [1995]. They also demonstrated a strong correlation between the optical b2i and the inclination of the magnetic field as measured at GOES 8 and developed an empirical model for predicting the GOES 8 inclination. *Nicholson et al.* [2002] used data obtained from MSPs located at Gillam and Fort Smith, Canada, and Poker Flat, Alaska, and demonstrated that ground-based MSPs are capable of obtaining a large number of simultaneous boundary determinations.

[5] Satellite-based observations of the proton aurora (and thus of the proton IB) were so far restricted to in situ satellite particle detection. Until the launch of the IMAGE satellite, no capability existed for global remote sensing of the proton aurora. Consequently, the IB sampling was spatially and temporally restricted. To overcome this limitation, we propose to use global data obtained with the FUV spectrographic proton imager (SI12) on board IMAGE that provide snapshots of proton precipitation with a 2-min resolution. Since the launch of the IMAGE satellite in March 2000, the FUV instrument provides the capability to simultaneously observe the aurora in three spectral bands:

[6] 1. The Wideband Imaging Camera (WIC) observes the aurora in a broad (1350-1700 Å) ultraviolet band sensitive mainly to Lyman-Birge-Hopfield N₂ bands and NI lines.

[7] 2. The SI12 spectral imager isolates a narrow region (2 Å) with a peak sensitivity at 1218 Å and images Doppler-shifted Ly α auroral emission.

[8] 3. The SI13 spectral imager selects a 50 Å passband centered on the O I 1356 Å feature.

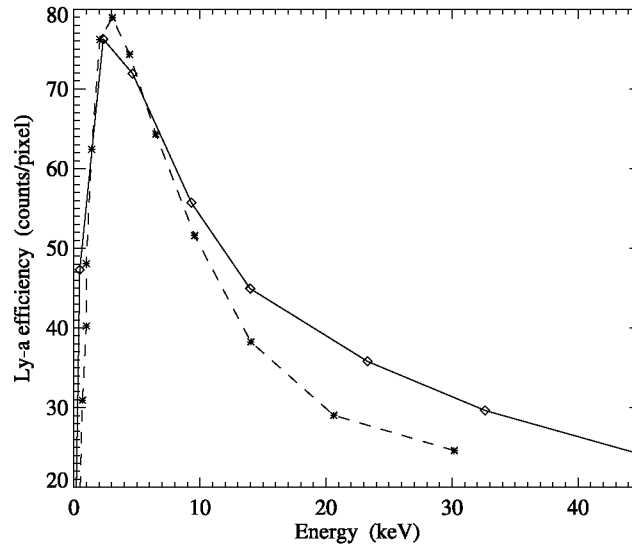
[9] The responsivity of these instruments was validated by laboratory and in-flight calibrations using hot stars and is updated daily [Frey *et al.*, 2003].

[10] SI12 is designed to monitor the global-scale proton precipitation. It includes a grill system to reject the intense (>10 kR) geocoronal Ly α emission at 1215.6 Å, which would otherwise appear as an impenetrable diffuse glow, and to isolate a fraction of the Doppler-broadened auroral Ly α line profile [Mende *et al.*, 2000a, 2000b]. Since this emission is emitted by excited fast hydrogen atoms, the line profile for a given observation geometry depends on the energy spectrum of the incident auroral protons and their pitch angle distribution. In addition, the response of the SI12 instrument with its multiple pass-bands depends on the Ly α line profile [Gérard *et al.*, 2001]. The shape of this profile is also influenced by the orientation of the line of sight with respect to the local magnetic field lines. Ideally, one would like to obtain a direct relationship between the observed instrumental count rate and the precipitated proton energy flux. However, the complexity of the atmospheric and instrumental processes involved makes it necessary to simulate the SI12 response for a range of parameters describing the proton precipitation and the geometry of the observations. The most relevant form of calibration included the observation of aurora with simultaneous FAST spacecraft-based electron and ion flux measurements. The role of the proton characteristic energy and pitch angle distribution on the Ly α line profile was analyzed with a Monte Carlo direct simulation model [Gérard *et al.*, 2001]. Figure 1 shows the efficiency of the SI12 detector as a function of the mean energy for incident mono energetic protons (dashed line) and for a kappa function initial distribution (solid line). The drop in efficiency of the Ly α emission rate versus energy results from the increasing importance of other processes competing with excitation into the H(2p) state as the initial proton energy increases [Strickland *et al.*, 1993; Gérard *et al.*, 2000]. The emission rates are calculated for a nadir-viewing observation, assuming that the pixels are uniformly filled by the Ly α auroral emission. The instrument efficiency drops for low-energy proton precipitation owing to the lack of an extended red-shifted Ly α wing and for high-energy protons which spend proportionally more energy in ionization than in Ly α excitation processes. This rapidly varying sensitivity at low energies also limits the accuracy of the signal conversion into energy flux units.

[11] The proton energy fluxes are then obtained from the SI12 count rate using the calibrated relationship between the SI12 signal and the NOAA in situ measurements of proton precipitation [Coumans *et al.*, 2002]. This method was validated by comparisons with in situ measurements of the auroral particle energy flux obtained from FAST [Frey *et al.*, 2001; Gérard *et al.*, 2001; Bisikalo *et al.*, 2003], NOAA [Hubert *et al.*, 2002; Coumans *et al.*, 2002; Meurant *et al.*, 2003], and DMSP [Coumans *et al.*, 2004] satellites.

[12] In this study, we first examine the possibility of determining the location of the isotropy boundary from the latitude of the maximum proton precipitation observed by SI12 global data. For this purpose we compare the location of the IB determined from in situ particle measurements with that of the maximum proton precipitation observed with SI12. Since the IB is not directly detectable with the SI12 instrument, the objective in the second part of this study is to find a new indicator of the magnetic field line stretching, easily determined on the basis of SI12 images. We chose the maximum SI12 emission (MAX SI12) as a new reference and determined whether it is a good indicator of the amount of stretching of the magnetic field lines in the night sector.

Figure 1: Dependence of the calculated SI12 count rate (counts/pixel over a 5 s integration period) on the mean proton energy for the total Ly α nadir emission. The dashed line is for a monoenergetic (1 mW m^{-2}) proton precipitation, and the solid line is for a kappa function distribution.



2. Comparison Between SI12 and Low-Latitude Satellite IB Determination

2.1. DMSP-SI12 Comparison

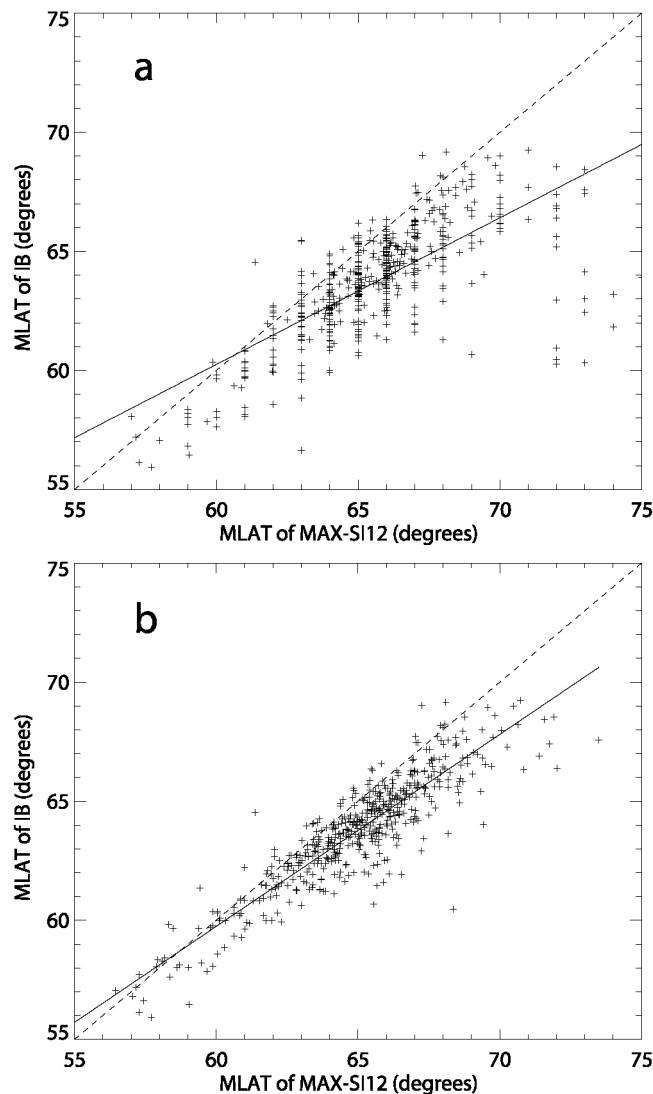
[13] To compare simultaneous DMSP and SI12 data, we selected a period for which SI12 data is most suitable for this study, i.e., a time interval when the IMAGE spacecraft was well positioned above the North Pole and during winter solstice to decrease contamination by reflected sunlight (very low at winter solstice). We thus chose a limited period, between 15 November 2000 and 31 January 2001. We considered all DMSP satellite crossings of the northern nightside auroral oval during this period and selected those where (1) the trajectory of the DMSP satellites is quasi-perpendicular to the auroral oval (the satellites having to reach at least 81° magnetic latitude (MLAT)); indeed, a trajectory too tangent to the oval can induce difficulties in locating the MLAT of b2i and the maximum SI12 emission, (2) no particular dynamical event such as a substorm or a shock-induced aurora was observed during the time interval 2 hours before and half an hour after the DMSP crossings (these dynamical and unusual situations will be studied in a future study), and (3) the IMAGE spacecraft is simultaneously well positioned so that it observes the entire DMSP trajectory between 52 and 81° MLAT.

[14] We thus obtained 519 simultaneous DMSP (F12, F13, F14, and F15) satellite and SI12 measurements. The DMSP satellites are quasi-polar Sun-synchronous satellites at a nominal altitude of 830 km with an orbital period of ~ 100 min. The orbits of all four DMSP satellites used in this study are confined to the evening sector (between 1700 and 2130 magnetic local time (MLT)) during the selected period. They carry the Special Sensor Precipitating Electron and Ion Spectrometer (SSJ/4) auroral particle spectrometers, which measure the electron and ion particle fluxes between 30 eV and 30 keV. The detectors are oriented toward the zenith and produce a complete spectrogram in the loss cone every second. The DMSP detectors provide energy spectra of electrons and ions every second in 20 logarithmically spaced energy channels extending from 30 eV to 30 keV. The positions of b2i are automatically derived from ion flux measurements [Newell *et al.*, 1996] and are assimilated to the isotropy boundary [Newell *et al.*, 1998].

[15] From the images obtained simultaneously with each DMSP crossing we extracted SI12 pixels along the footprint of the DMSP trajectory and constructed the intensity distribution with a time resolution of ~ 2 min. Thus, for each simultaneous DMSP and SI12 observation of the auroral nightside proton precipitation we compare the latitude of the b2i limit with the latitudinal profile of intensity (the maximum) of auroral emission observed by SI12 along the same trajectory. The ion energy flux measurements (ions from 2 to 12 keV to correspond with SI12 observations) from DMSP along its path are first smoothed on time on the basis of the SI12 point spread function. The IMAGE spacecraft pointing errors are then corrected by aligning the SI12 profile median with the median of the ion flux DMSP profile.

[16] The b2i limit is defined as the peak of the energy flux precipitation of ions from 3 to 30 keV observed by DMSP and is also frequently the equatorward limit of the proton precipitation. It is always distinct from the median of the ion flux DMSP profile. The maximum ion precipitation (MAX SI12) rarely coincides exactly with the median of the SI12 profile. Therefore aligning the SI12 profile median with the median of the ion flux DMSP profile does not influence the actual relative position between the b2i limit and the peak observed by SI12 (see section 2.3 and Figure 2). In this study, the procedure was automatic. For detailed studies of events without simultaneous DMSP data a visual inspection of the image and the coordinate grid based on IMAGE attitude data would be necessary, limiting the pointing error to less than 2° . *Newell et al.* [1998] showed that the b2i limit provides an excellent approximation to the IB limit. We now examine whether the maximum of the intensity of the ion precipitation observed by SI12 is appropriate to estimate the position of the IB.

Figure 2: (a) Comparison of isotropy boundary (IB) magnetic latitudes from the DMSP (519 measurements between 1700 and 2130 magnetic local time (MLT)) and NOAA 8 (181 measurements between 0200 and 0330 MLT) with simultaneous MAX SI12 (IMAGE) magnetic latitudes. The dashed line is the bisectrix, and the solid line is the linear best fit. (b) Same comparison except with corrected IMAGE data pointing uncertainties.



2.2. NOAA-SI12 Comparison

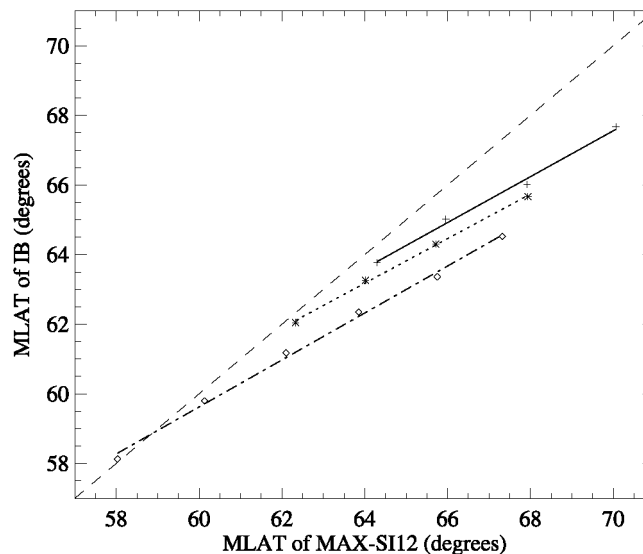
[17] As mentioned in section 2.1, during the period studied in this work (15 November 2000 to 31 January 2001), DMSP measurements were confined to one nightside MLT sector (between 1700 and 2130 MLT). We used in situ data from the polar Sun-synchronous NOAA 16 satellite at about 850 km to complement the

comparison with SI12 and to extend our comparison to other local times. NOAA 16 crosses the northern nightside auroral oval in the postmid-night sector (between 0200 and 0330 MLT). The same conditions required to select DMSP data were applied to select NOAA data. We used measurements of the precipitated flux (oriented radially upward within the loss cone) and of the locally trapped flux (as viewed perpendicular to the radial direction) of 30 to 80 keV protons. These data were collected with a medium energy proton and electron detector (MEPED) instrument with a time resolution of 2 s, but we used 16-s-averaged bins. We selected the time interval from November 2001 to January 2002, covering a winter solstice period. We applied an automatic method to determine the IB for the selected NOAA 16 orbits. It is based on the ratio of precipitated flux I_0 to trapped flux I_{90} of 30-80 keV protons. The algorithm proceeds from low to higher latitudes and locates the IB where the I_0/I_{90} ratio becomes greater than 0.9 or jumps from less than 0.4 to greater than 0.75 in less than 32 s. This procedure eliminates cases for which the IB was found poleward of the maximum of precipitated flux.

2.3. IB and MAX SI12 Relative Positions

[18] We chose the latitude of the SI12 maximum signal as a proxy of the IB and the magnetic field stretching since it is easily identified and unambiguously determined from the images. Figure 2 compares the latitude of the b2i limit with that of MAX SI12 observed in the evening (morning) sector simultaneously by DMSP (NOAA) and SI12, respectively. This comparison is made without (Figure 2a) and with (Figure 2b) the correction of the pointing IMAGE uncertainties mentioned before, and it shows that this correction largely improves but does not change the correlation. With the dashed line being the bisectrix, one immediately notices that b2i is almost always located at a lower latitude than the maximum of SI12 intensity. The isotropy boundary appears to be very close to the maximum when precipitation occurs at low latitude ($<60^\circ$ MLAT), while the isotropy boundary is observed more than 2° away from MAX SI12 when precipitation occurs at higher latitude ($>70^\circ$ MLAT). We did not account for the fact that the energy of the observed protons is not necessarily identical in the SI12 images and in the DMSP and NOAA data. SI12 mainly responds to protons between ~ 1 and ~ 12 keV (Figure 1), while DMSP observes all proton energies up to 30 keV and NOAA observes all proton energies up to 80 keV. Numerical simulation [Sergeev *et al.*, 1983] and NOAA observations [Newell *et al.*, 1998] show that the latitude of the isotropy boundary is found at about 1.5° more poleward for 1 keV protons than for 30 keV protons and at about 2° more poleward than for 80 keV protons. Therefore the shift observed between MAX SI12 and the IB may be partly due to this effect. The statistical energy range of protons in the nightside sector (between 2200 and 0200 MLT) between 62 and 65° MLAT (MAX SI12 is situated between 63.5 and 65° MLAT in this MLT sector) is, according to Hardy *et al.*'s [1989] model, somewhat higher than the energy range observed with the SI12 imager. It ranges between 0.8 and 17.7 keV for $Kp = 0$ and 3.9 and 20.4 keV for $Kp = 3$.

Figure 3: Same plot as Figure 2 except the data have been binned on 1° MLAT intervals and divided into three groups. Crosses and solid line correspond to $AE < 150$, stars and dotted line correspond to $150 < AE < 300$, and diamonds and dot-dashed line correspond to $AE > 300$.



[19] The linear regression in Figure 2b gives a large correlation coefficient ($r = 0.91$) between the latitude of the b2i limit and that of MAX SI12. Some of the discrepancies with DMSP b2i are possibly due to incorrect automatic determination of the DMSP boundaries as experienced during this study. We also find that the scatter is controlled by different parameters, mainly the activity index AE and the magnetic local time considered.

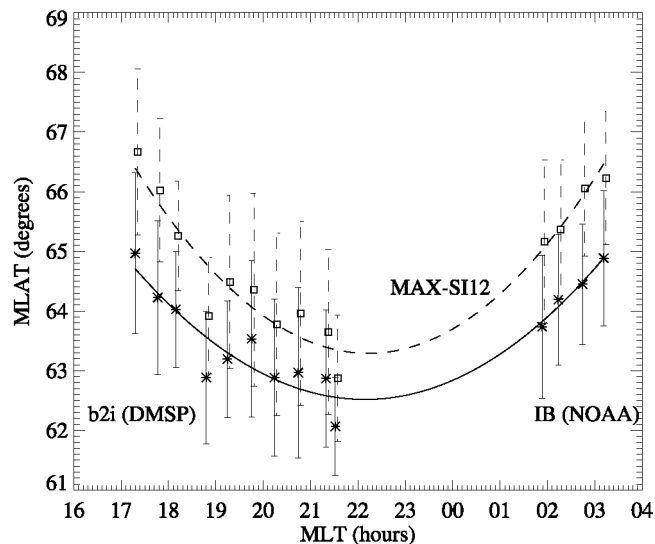
2.3.1. Magnetic Activity Index AE

[20] In Figure 3 we again compare the latitudes of the b2i limit and MAX SI12, but the observations are sorted out into three classes of AE values corresponding to quiet, moderate, and high levels of auroral electrojet activity. The three groups correspond to $AE < 150$, $150 < AE < 300$, and $300 > AE$, respectively. The dashed line is the bisectrix, where b2i and MAX SI12 coincide. The data have been binned on 1° intervals of magnetic latitude. The plots show that the distance between b2i and the maximum depends on the AE index: b2i is closest to the maximum at $\sim 63^\circ$ MLAT for quiet magnetic conditions ($AE < 150$) and at $\sim 59^\circ$ MLAT for $AE > 300$. In other words, at the same latitude, b2i is closer to the maximum when the magnetic activity is weak.

2.3.2. Magnetic Local Time

[21] We now examine the variation of the b2i-MAX SI12 distance with magnetic local time. The observations are first grouped into 0.5-hour MLT bins. For each group, Figure 4 shows the MLAT average value of MAX SI12 (squares and dashed lines) and the IB (stars and solid lines) as a function of the mean MLT, together with the standard deviation. Figure 4 shows that the latitude of the two limits varies with local time as well as, to some extent, the distance between these limits. MAX SI12 exhibits the same dependence on MLT as the isotropy boundary. The asymmetry with respect to 0000 MLT previously observed for the IB in the nightside by *Sergeev et al.* [1997] and *Newell et al.* [1998] is also present for the maximum of proton emission (MAX SI12). The two binomial fits shown in Figure 4 are centered on 2210 and 2215 MLT for IB and MAX SI12, respectively. The statistical distance between these fitted curves varies with the MLT considered; it increases from 0.8° MLAT at 2200 MLT to 1.7° MLAT at 1700 MLT (1.6° MLAT at 0300 MLT).

Figure 4: IB magnetic latitude (stars and solid lines) from DMSP (519 measurements) and NOAA 16 (181 measurements) and MAX SI12 (IMAGE) magnetic latitude (squares and dashed lines) as a function of MLT. The vertical bars correspond to the standard deviation of each bin.



3. MAX SI12 Latitude and Magnetic Field Line Stretching

3.1. B Field Elevation Data

[22] We now compare MAX SI12 with the magnetic field orientation measured simultaneously at geosynchronous distance at the same MLT by the magnetometer on board GOES 8. The GOES satellites carry a magnetometer providing continuous measurements of the Earth's magnetic field components B_P , B_E , and B_N . B_P is parallel to the satellite spin axis, which is perpendicular to the satellite's orbital plane. B_E lies parallel to the satellite-Earth center line and points earthward. B_N is perpendicular to both H_P and H_E and points eastward for GOES 8. Field strength changes as small as 0.2 nT can be measured. To evaluate the magnetic stretching in the geotail, we use the magnetic field elevation angle in the solar magnetic coordinate system, defined as $E1 = \arctan(B_P/B_E)$. We used 1-min-averaged magnetic field measurements provided by the GOES 8 satellite, which is geosynchronous at $\sim 10.8^\circ\text{N}$ MLAT. For a dipolar magnetic field at magnetic latitude λ the inclination angle I_{dip} is given by

$$\tan I_{\text{dip}} = 2 \tan \lambda.$$

We find a value of 69.12° for the dipolar elevation angle $E1_{\text{dip}}$, i.e., the elevation angle which GOES 8 would measure if the geomagnetic field were dipolar. This $E1_{\text{dip}}$ value is therefore the limit below which the magnetic field lines are stretched (in the nightside) and beyond which they are compressed (in the dayside).

[23] The GOES magnetometer data are subject to diurnal and seasonal variations stemming from the variations of the position of the neutral sheet with respect to the satellite. *Skone et al.* [1995] processed the data to remove seasonal effect by using the semiempirical expression developed by *Lopez* [1990] expressing the displacement of the neutral sheet with respect to the magnetic equatorial plane. In this study, we do not compare different seasons, and each month is analyzed separately. For this comparison we use 31 GOES 8 orbits in December 2000. Figure 5 shows all the elevation angles measured by GOES 8 during December 2000 and their dependence on the satellite magnetic local time. The dashed line indicates the value of a dipolar limit. It clearly appears that the magnetic field is usually compressed in the noon sector and is always stretched in the midnight sector.

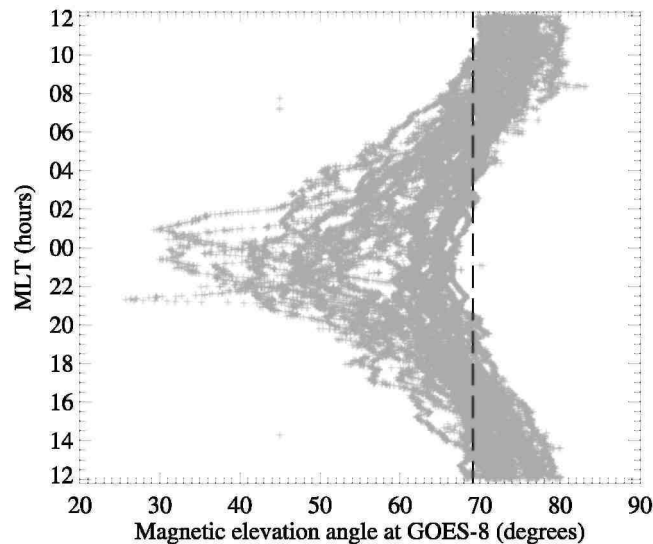
3.2. GOES-SI12 Data Comparison

[24] GOES satellites record 1-min-averaged values of the geomagnetic field components, each associated with a specific UT and MLT. Each one of these measurements can be correlated to the simultaneous SI12 image when such an image exists, that is, if the IMAGE satellite is well positioned to observe the point of the auroral oval corresponding to the same magnetic field line. We extract the observation at the MLT of the field line footprint and determine the latitude and the intensity of the maximum SI12 auroral emission across a cut at the GOES MLT. We then compare the magnetic elevation angle measured by GOES 8 in December 2000 in the midnight sector (between 2300 and 0100 MLT) with the corresponding MAX SI12 magnetic latitude (Figure 6a). Figure 6b shows a similar comparison for February 2001. Figure 6 shows that for very stretched magnetic field lines the proton precipitation takes place at lower latitudes than when the magnetic field lines are quasi-dipolar. The dashed line is the dipolar limit. We also observe that the latitude of the maximum auroral ion precipitation is strongly correlated with the geotail stretching in the nightside. The linear regression has a correlation coefficient $r = 0.84$ in Figure 6b. However, we note that a linear regression does not necessarily provide the best possible fit for large values of the elevation angle. Indeed, a saturation effect is observed when the field lines are moderately stretched in a quasi-dipolar configuration, since near midnight the solar wind flow is such that it is unlikely to observe an elevation angle exceeding the dipolar limit. The thin dash-dotted line in Figure 6a shows the linear regression obtained by *Sergeev and Gvozdevsky* [1995] between the MT index and the elevation angle. The MT index is defined as the invariant latitude of the isotropy boundary of ~ 100 keV protons reduced to the midnight meridian. The mean distance between the MT index and our best fit is 0.8° MLAT, which is what we found in Figure 4 between the IB and MAX SI12 at midnight.

[25] Figure 7 shows the relationship between the maximum SI12 count rate (MAX SI12) and the elevation angle measured by GOES 8 for the same field line in December 2000 (Figure 7a) and February 2001 (Figure 7b). The comparison indicates that MAX SI12 intensity also covaries with the level of magnetic field line stretching. In the nightside a stretched magnetosphere generally corresponds to a higher auroral proton-precipitated flux. This result is particularly interesting, since it confirms that the brightness of proton diffuse auroras, as well as the stretching of the magnetic field lines in the inner magnetosphere, is both due to a larger current-carrying ability caused by heating of the magnetospheric plasma. A stretched magnetic field implies more equator-ward aurora

because the isotropic boundary in the equatorial plane is closer to the Earth. Therefore a stronger plasma sheet pressure causes a more stretched field in the inner magnetosphere and equatorward and brighter proton auroras. Moreover, with increasing stretching, the isotropy boundary moves inward into a region where larger proton energy flux is now available to be precipitated. Inversely, following magnetic field depolarization, the isotropy boundary moves outward into the region with smaller available proton energy flux, causing the decrease of maximum precipitating flux. The results described above show that in the midnight sector the location and the intensity of the proton precipitation are both largely correlated with the amount of magnetic field line stretching. We now examine if these correlations remain present when moving away from 0000 MLT. Away from the midnight sector a good correlation is still observed inside of the 2000 to 0400 MLT sector. Farther away from midnight the correlation drops off drastically. This result is expected considering that only near midnight is the equatorial position of the IB near the geostationary orbit (the theoretical IB is located at the equator at distance 5-9 R_E , smaller distances corresponding to the increasing tailward stretching of the magnetic field [Sergeev and Gvozdevsky, 1995]). Their relative distance rapidly increases away from midnight. Therefore, at local times later than 4 hours away from midnight the magnetic field measured by GOES is no longer indicative of the field that actually controls the IB location.

Figure 5: Elevation angle measured by GOES 8 in December 2000 according to the MLT location of the GOES 8 spacecraft. The dashed line corresponds to the dipole limit.



3.3. Time Evolution

[26] We now examine the time evolution of the elevation angle at geosynchronous distance and the concurrent location and intensity of the proton precipitation. Figure 8 shows an example of the temporal sequence of simultaneous SI12 (crosses and diamonds) and GOES 8 (dashed line) observations from 1200 UT, 4 December 2000 to 1200 UT, 5 December 2000. Superimposed on the diurnal variation of the magnetic elevation angle, we note a brief and localized drop of the elevation angle (between the two vertical solid bars) when GOES 8 is between 1730 and 1830 MLT (at this MLT, GOES 8 is not at the most favorable position, and the disturbance appears small), with a simultaneous enhancement of the *AE* index (dotted line). This increase of *AE* did not correspond to a sub-storm initiation, as the analysis of SI12 images shows a weak intensification located between 2200 and 2300 MLT lasting only about 10 min. Moreover, this intensification is not triggered by the relaxation of the magnetic field lines, as it would be for substorms, but increases simultaneously with the stretching of the magnetic field lines. Furthermore, no evident trigger of a shock-induced aurora or a substorm was found in the solar wind characteristics. The cause of the stretching is not crucial in this context; the relevant result is that this magnetic disturbance did not occur without a modification of the proton auroral morphology and brightness as seen by SI12. Indeed, the latitude of MAX SI12 decreases as the elevation angle drops off (i.e., when stretching increases), and MAX SI12 is simultaneously enhanced. Later, when the magnetic field lines relax, the latitude of MAX SI12 moves up, and its intensity drops off to a smaller value than before the magnetic disturbance. This

time behavior of the elevation angle, the latitude, and the intensity of MAX SII2 confirm the self-consistent evolution between the state of the geotail field lines (and their curvature) and the strength and latitudinal distribution of proton precipitation in the nightside. Particle simulations [Sergeev *et al.*, 1983] indicate that a drop of curvature radius to gyroradius ratio ($R = R_c/\rho$) locally increases the rate of the loss cone precipitation only if R decreases from $R > 8$ to $R < 8$ values. Instead, if it remains in the $R \ll 8$ domain, no increase of precipitation will follow.

Figure 6: Comparison between the value of the magnetic elevation angle (GOES 8) and the simultaneous MAX SII2 magnetic latitude (IMAGE) in (a) December 2000 and (b) February 2001. The dashed line corresponds to the dipole limit. The thin dash-dotted line in Figure 6a shows the linear regression obtained by Sergeev and Gvozdevsky [1995] between the MT index and the elevation angle. The MT index is defined as the invariant latitude of the isotropy boundary of ~ 100 keV protons reduced to the midnight meridian.

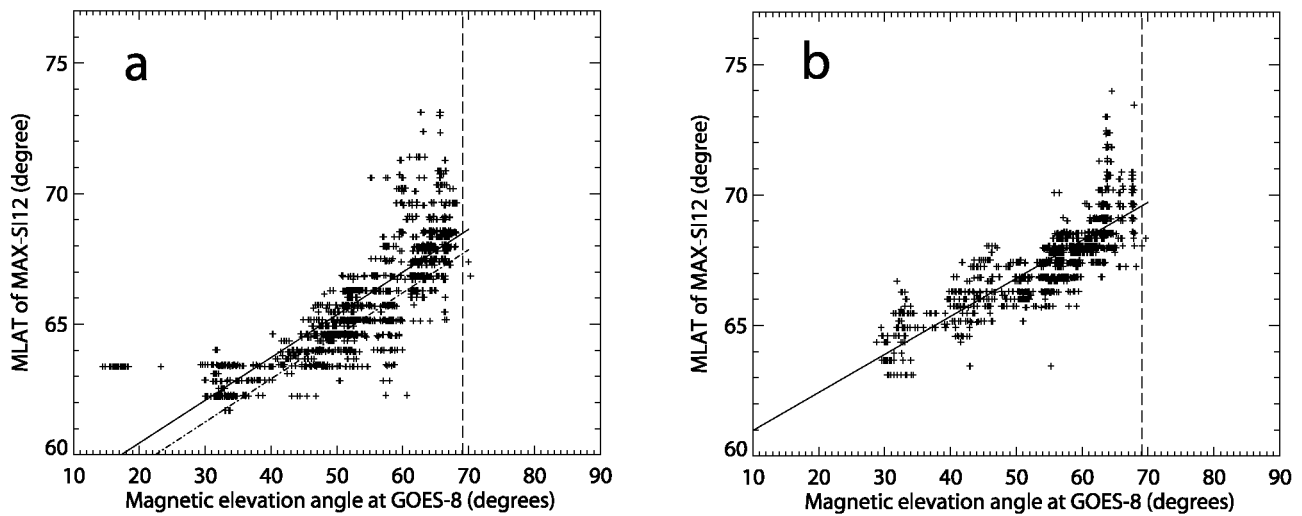


Figure 7: Comparison between the value of the magnetic elevation angle (GOES 8) and the simultaneous MAX SII2 intensity (IMAGE) in (a) December 2000 and (b) February 2001. The dashed line corresponds to the dipole limit.

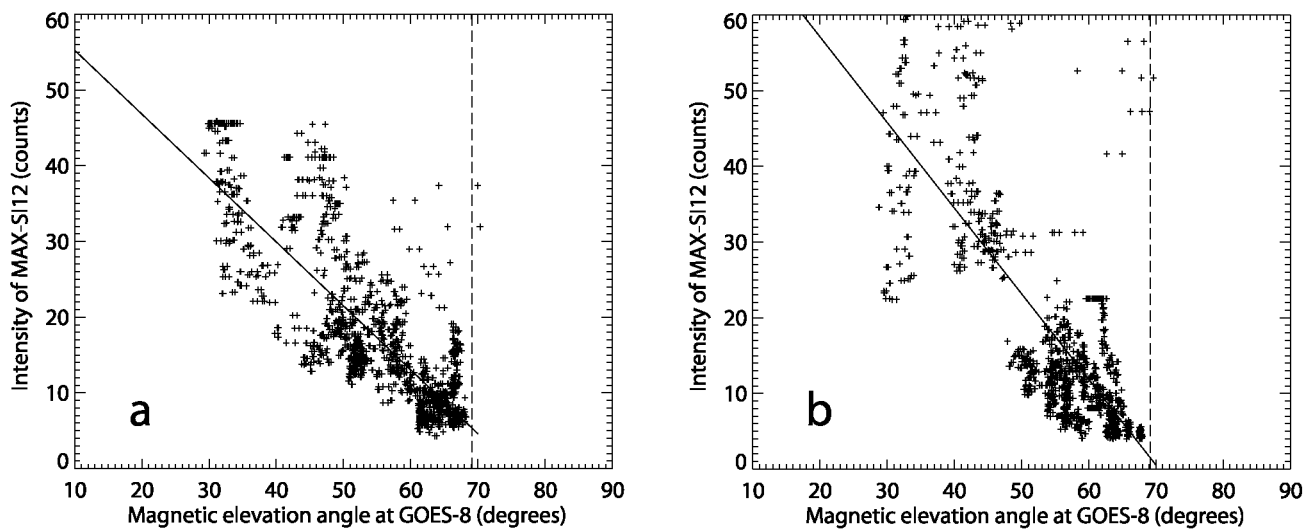
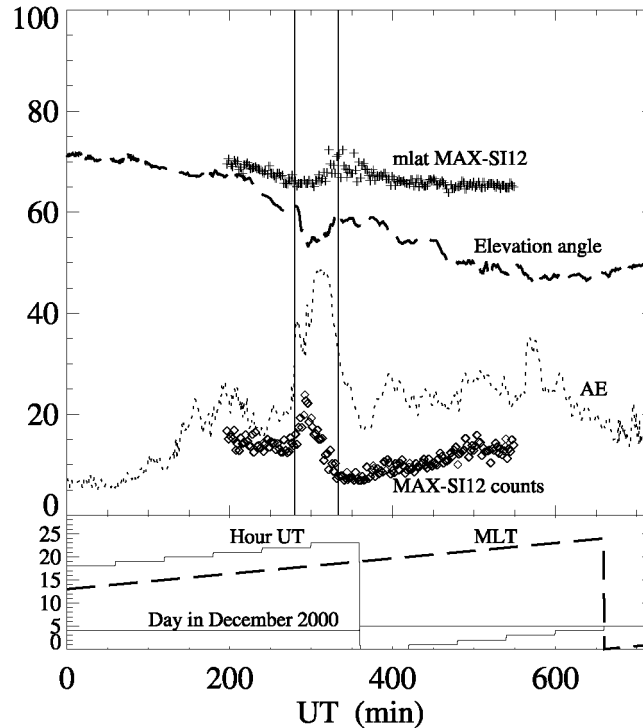


Figure 8: Example of time evolution between MAX SI12 and the magnetic field line stretching, (top) Elevation angle (dashed line) of the magnetic field resulting from GOES 8 measurements from 1800 UT, 4 December 2000 to 0600 UT, 5 December 2000. The crosses and diamonds represent the magnetic latitude and the intensity of MAX SI12, respectively, at the same MLT as for GOES 8. The dotted line shows the AE index divided by 10. (bottom) Day, hour UT, and the MLT (dashed line).



4. Summary and Conclusions

[27] We show the latitude of the isotropy boundary may be determined, using SI12 global data, from the latitude of the maximum proton precipitation observed by this instrument. Parameters such as the magnetic local time and the magnetic activity index AE exert control on this location. This first result coupled with the study of *Sergeev and Gvozdevsky* [1995] leads us to suggest that a direct relation exists between MAX SI12 and the magnetic elevation angle. Indeed, we also show that MAX SI12, as well as the IB, is a good indicator of the stretching of the magnetic field lines. We find the same level of correlation ($r \sim 0.9$) and a similar standard deviation ($\sigma = 0.89$) as was obtained by *Sergeev and Gvozdevsky* [1995] on the basis of in situ measurements. Both the IB and MAX SI12 are, unlike the usual global activity indices (magnetic indices like AE , Kp , Dst), well suited to predict the instantaneous magneto spheric configuration in the midnight sector. The agreement between the location of MAX SI12 and the magnetic elevation angle measured at geosynchronous distance decreases away from the midnight sector. Presumably, there is an equally strong connection between the stretching of the magnetic field lines and the latitude of MAX SI12 at all local times. However, the isotropic region in the equatorial plane is presumably farther out, so that the correlation with geosynchronous measurements decreases. The IMAGE satellite performs global remote sensing of the proton aurora over a long continuous time interval. The latitude of MAX SI12 is thus similar to the IB, but it makes it possible to follow the dynamic evolution of the magnetic field lines on a global scale. Finally, we show that even brief and localized magnetic field perturbations (even observed at ~ 1800 MLT, where GOES 8 is not at the most favorable position) evolve self-consistently with the proton auroral morphology and brightness and are also observed with the SI12 imager. The response of these perturbations detected by SI12 occurs simultaneously with the magnetic field disturbances. Therefore MAX SI12 also provides a time history of the perturbations. In the future this method will provide a tool to study the global topology of magnetic field lines and their movements and distortions in relation to solar wind conditions.

[28] **Acknowledgments.** J.C.G. and B.H. are supported by the Belgian National Fund for Scientific Research (FNRS), and V.C. is supported by a fellowship from the Belgian Fund for Research in Industry and Agriculture (FRIA). The IMAGE FUV investigation was supported by NASA through SWRI subcontract 83820 at the University of California, Berkeley, contract NAS5-96020. This work was funded by the PRODEX program of the European Space Agency (ESA) and the Fund for Collective and Fundamental Research (FRFC grant 2.4517.02). *AE* indices are provided by the World Data Center for Geomagnetism (WDC-C2) in Kyoto (<http://swdcwww.kugi.kyoto-u.ac.jp/aedir/>). We acknowledge data providers H. Singer at NOAA SEC and CDAWeb for the GOES data and D. Evans at NOAA SEC for the NOAA data. The DMSP particle detectors were designed by Dave Hardy of AFRL, and data were obtained from JHU/ APL. We thank Dave Hardy, Fred Rich, and Patrick Newell for the use of the particle detectors. We thank both reviewers for useful suggestions.

[29] Arthur Richmond thanks Eric Donovan and Victor Sergeev for their assistance in evaluating this paper.

References

- Bisikalo, D. V., V. I. Shematovich, J.-C. Gérard, M. Meurant, S. B. Mende, and H. U. Frey (2003), Remote sensing of the proton aurora characteristics from IMAGE-FUV, *Ann. Geophys.*, *21*, 2165.
- Coumans, V., J.-C. Gérard, B. Hubert, and D. S. Evans (2002), Electron and proton excitation of the FUV aurora: Simultaneous IMAGE and NOAA observations, *J. Geophys. Res.*, *107*(A11), 1347, doi:10.1029/2001JA009233.
- Coumans, V., J.-C. Gérard, B. Hubert, M. Meurant, and S. B. Mende (2004), Global auroral conductance distribution due to electron and proton precipitation from IMAGE-FUV observations, *Ann. Geophys.*, *22*, 1595.
- Donovan, E. F., B. J. Jackel, I. Voronkov, T. Sotirelis, F. Creutzberg, and N. A. Nicholson (2003), Ground-based optical determination of the b2i boundary: A basis for an optical MT-index, *J. Geophys. Res.*, *108*(A3), 1115, doi:10.1029/2001JA009198.
- Frey, H. U., S. B. Mende, C. W. Carlson, J.-C. Gérard, B. Hubert, J. Spann, R. G. Gladstone, and T. J. Immel (2001), The electron and proton aurora as seen by IMAGE-FUV and FAST, *Geophys. Res. Lett.*, *28*, 1135.
- Frey, H. U., S. B. Mende, T. J. Immel, J.-C. Gérard, B. Hubert, S. Habraken, J. Spann, G. R. Gladstone, D. V. Bisikalo, and V. I. Shematovich (2003), Summary of quantitative interpretation of IMAGE far ultraviolet auroral data, *Space Sci. Rev.*, *109*, 255.
- Gérard, J.-C., B. Hubert, D. V. Bisikalo, and V. I. Shematovich (2000), A model of the Lyman *a*. line profile in the proton aurora, *J. Geophys. Res.*, *105*, 15,795.
- Gérard, J.-C., B. Hubert, M. Meurant, V. I. Shematovich, D. V. Bisikalo, H. Frey, S. Mende, G. R. Gladstone, and C. W. Carlson (2001), Observation of the proton aurora with IMAGE FUV imager and simultaneous ion flux in situ measurements, *J. Geophys. Res.*, *106*, 28,939.
- Hardy, D. A., M. S. Gussenhoven, and D. Brautigam (1989), A statistical model of auroral ion precipitation, *J. Geophys. Res.*, *94*, 370.
- Hubert, B., J.-C. Gérard, D. S. Evans, M. Meurant, S. B. Mende, H. U. Frey, and T. J. Immel (2002), Total electron and proton energy input during auroral substorms: Remote sensing with IMAGE-FUV, *J. Geophys. Res.*, *107*(A8), 1183, doi:10.1029/2001JA009229.
- Lopez, R. (1990), The position of the magnetotail neutral sheet in the near-Earth region, *Geophys. Res. Lett.*, *17*, 1617.
- Mende, S. B., et al. (2000a), Far ultraviolet imaging from the IMAGE spacecraft. 1. System design, *Space Sci. Rev.*, *91*, 243.
- Mende, S. B., et al. (2000b), Far ultraviolet imaging from the IMAGE spacecraft. 2. Wideband FUV imaging, *Space Sci. Rev.*, *91*, 211.
- Meurant, M., J.-C. Gérard, B. Hubert, V. Coumans, V. I. Shematovich, D. V. Bisikalo, D. S. Evans, G. R. Gladstone, and S. B. Mende (2003), Characterization and dynamics of the auroral electron precipitation during substorms deduced from IMAGE-FUV, *J. Geophys. Res.*, *108*(A6), 1247, doi:10.1029/2002JA009685.
- Newell, P. T., Y. I. Feldstein, Y. I. Galperin, and C.-I. Meng (1996), Morphology of nightside precipitation, *J. Geophys. Res.*, *101*, 10,737.
- Newell, P. T., V. A. Sergeev, G. R. Bikkuzina, and S. Wing (1998), Characterizing the state of the magnetosphere: Testing the ion precipitation maxima latitude (b2i) and the ion isotropy boundary, *J. Geophys. Res.*, *103*, 4739.
- Nicholson, N. A., E. F. Donovan, B. J. Jackel, I. Voronkov, L. L. Cogger, D. Lummerzheim, F. Creutzberg, and T. Sotirelis (2002), Using the optical b2i as a tool for event timing, paper presented at the 6th International Conference on Substorms (ICS-6), NASA, Seattle, Wash., 25-29 Mar.
- Sergeev, V. A., and B. B. Gvozdevsky (1995), MT-index—A possible new index to characterize the magnetic configuration of magnetotail, *Ann. Geophys.*, *13*, 1093.

Sergeev, V. A., E. M. Sazhina, N A. Tsyganenko, J. A. Lundblad, and F. Soraas (1983), Pitch-angle scattering of energetic protons in the magnetotail current sheet as the dominant source of their isotropic precipitation into the nightside ionosphere, *Planet. Space Sci*, 31, 1147.

Sergeev, V. A., G R. Bikkuzina, and P. T. Newell (1997), Dayside isotropic precipitation of energetic protons, *Ann. Geophys.*, 15, 1233.

Skone, S. H., E. F. Donovan, and G Rostoker (1995), Characterizing the quiet time magnetic field at geostationary orbit, *J. Geophys. Res.*, 100, 23,583.

Strickland, D. J., R. E. Daniell Jr., J. R. Jasperse, and B. Basu (1993), Transport-theoretic model for the electron-proton-hydrogen atom aurora: 2. Model results, *J. Geophys. Res.*, 98, 21,533.